Hindawi
Advances in Civil Engineering
Volume 2019, Article ID 7286284, 13 pages
https://doi.org/10.1155/2019/7286284

Research Article

Constant Ductility Site-Specific Yield Point Spectra for Seismic Design

Duofa Ji[1,2], **Weiping Wen**[1,2] **and Changhai Zhai**[1,2]

[1]*Key Lab of Structures Dynamic Behavior and Control of the Ministry of Education, Harbin Institute of Technology, Harbin 150090, China*
[2]*Key Lab of Smart Prevention and Mitigation of Civil Engineering Disasters of the Ministry of Industry and Information Technology, Harbin Institute of Technology, Harbin 150090, China*

Correspondence should be addressed to Weiping Wen; wenweiping@hit.edu.cn

Received 16 May 2019; Revised 22 July 2019; Accepted 29 July 2019; Published 14 August 2019

Academic Editor: Giuseppe Quaranta

Displacement-based seismic design (DBSD) is an iterative process because the strength and stiffness of a structure are needed to be adjusted in order to achieve a specific performance level, which is extremely inconvenient for designers in practice. Yield point spectra-based seismic design is treated as an alternative design method in which yield displacement as a basic parameter will not lead to an iterative process even though the lateral strength or stiffness of a structure changes during the whole design process. Along this line, this study focuses on investigating the yield point spectra (YPS) for structures located at different soil sites. YPS are computed for EPP systems under 601 earthquake ground motions. YPS for four soil sites are quantitatively analyzed by considering the influence of the vibration period, ductility factor, damping ratio, postyield stiffness ratio, and P-delta effect. The results indicate that compared with the effects of the damping ratio, the effects of the postyield stiffness ratio and P-delta effect on YPS are more profound. Finally, a prediction equation is proposed accounting for four soil sites and six ductility factors.

1. Introduction

In force-based seismic design, the deformation and energy dissipation capacity of structures are insufficient when subjected to large earthquake excitations, which is confirmed by postearthquake field reconnaissance [1, 2]. Thus, structures need to satisfy multiple performance objectives when subjected to different intensities of earthquake ground motions; that is, there is a need for performance-based seismic design (PBSD) that aims to mitigate the impact of earthquake disasters in terms of structural damage, economic losses, and casualties [3]. One widely used form of PBSD is displacement-based seismic design (DBSD) in which the displacement is adopted as the performance objective [4, 5].

In the early 1960s, Muto et al. [6] considered the displacement index in earthquake resistance design. In their investigation, they thought that the maximum inelastic displacement and maximum elastic displacement are very close for the same initial condition, and the engineers can design structures based on that assumption. On the contrary, Veletsos and Newmark [7] computed the structural strength demand by considering the combination of displacement and ductility demand. After that, Moehle [8, 9] simplified the multiple-degrees-of-freedom (MDOF) structures to equivalent single-degree-of-freedom (SDOF) systems and estimated the maximum displacement of MDOF structures based on the results of the displacement response spectra. Until the 1990s, DBSD [10–13] was proposed instead of force-based seismic design.

In the process of DBSD, the vibration period is treated as a basic parameter, and thus, designers need firstly to estimate the structural vibration period based on the type and size of the structure. Then, the strength and stiffness of the structure are needed to be adjusted until a specific performance level is reached. However, the above process will obviously cause the

final vibration period to be different from the former one and also cause changes to the structural seismic demand. Hence, DBSD is an iterative process that is extremely inconvenient for designers in practice [14, 15].

Along this line, Aschheim and Black [16] propose an alternative design method, yield point spectra (YPS), which treats yield displacement as a basic parameter. YPS characterize the relationships between the yield strength coefficient and yield displacement for structures under earthquake excitations. The authors investigated the seismic response of a moment-resistant frame and found that the yield displacements remained constant when the lateral strength or stiffness changed. The latter indicates that the selection of yield displacement as a basic parameter will not lead to an iterative process even though the lateral strength or stiffness of a structure changes during the whole design process. In YPS-based seismic design, the designers can first determine the area, allowing for seismic design, through YPS, for a specific performance level. Then, yield displacement can be estimated based on the geometric size and type of the structure. Finally, the strength of the structure can be determined in the corresponding area through YPS. Besides, YPS can be used for seismic assessment and rehabilitation because they can conveniently estimate the structural maximum displacement under earthquake excitations.

YPS were applied to design different types of structures such as structural components [17], reinforced concrete (RC) wall buildings [18, 19], coupled walls [20], and moment-frame structures [21]. For example, a 4-story moment-frame structure was designed based on yield point design spectra [21], and the results showed that the structure satisfied the performance limits of the system ductility and interstory drift. Tsiavos and Stojadinović [19] proposed a procedure for the seismic evaluation of existing structures by using the relation between the yield strength and displacement of the corresponding SDOF system, and the results were verified by comparing them with the experimental results of a 3-story RC shear wall structure. Besides, YPS can also be used to design structures having P-delta effect issues [22]. The authors illustrated the seismic design of a single bridge column with explicit consideration of P-delta effects and pointed out that the YPS's design results satisfy the performance limits of the system ductility and drift with no iterations, while five iterations were needed to obtain an acceptable design for the structural first-order demand by inelastic response spectra. On the contrary, Bozorgnia et al. [23] attempted to extend yield displacement and inelastic displacement spectra into probabilistic seismic hazard analysis (PSHA) by proposing a ground motion prediction equation (GMPE) for the yield strength coefficient and maximum inelastic displacement considering the source, path, and site parameters. Besides, the yield strength coefficient is also a core parameter in other seismic designs, e.g., [24, 25].

In the current YPS-based seismic design, YPS are determined by considering R-μ-T or R-C_1-T relationships that are defined in current seismic codes [26–28]. However, no specific yield strength coefficient-yield displacement, C_y-Δ_y, relationship can be found in the literature and seismic codes except the ones [17, 22] that only consider one selected ground motion, i.e., the 1940 El Centro earthquake record. Furthermore, the characteristics of YPS are not clear. Thus, there is a need to analyze the characteristics of YPS and formulate a C_y-Δ_y relationship.

Along these lines, the objective of this study is to understand the characteristics of YPS based on parametric analysis and to propose the C_y-Δ_y relationship based on statistical results. A total of 601 earthquake ground motions are selected from major global earthquakes. YPS are studied by considering the influence of the damping ratio, postyield stiffness ratio, and P-delta effect. Finally, a prediction equation that can be used in YPS-based seismic design is provided.

2. Definition of Energy Response Parameters

In general, there is a need to define the yield point of an SDOF system before plotting YPS. For example, the yield point is defined by the yield displacement, Δ_y, and the yield force, F_y, as shown in Figure 1. The ratio of the yield force, F_y, to the weight of the structure, W, is the yield strength coefficient, C_y. The analytical expression for C_y is provided as follows:

$$C_y = \frac{F_y}{W} = \frac{F_y}{mg} = \frac{4\pi^2 \Delta_y}{T^2 g}, \tag{1}$$

where m is the mass of the structure, g is the gravity acceleration, and T is the vibration period.

The yield strength coefficient, C_y, was calculated for an SDOF system with a specific ductility, defined herein as the ductility factor, μ, on the basis of the following equation:

$$\mu = \frac{\Delta_m}{\Delta_y}, \tag{2}$$

where Δ_m is the maximum inelastic displacement demand of the structure when subjected to earthquake ground motions.

Unlike other spectra that present the values of response indices versus vibration period, YPS plot the values of C_y versus Δ_y for constant-ductility SDOF systems considering a wide range of vibration periods. Herein, 120 SDOF systems are modeled with vibration periods, T, ranging from 0.05 to 6.00 s with a period increment of 0.05 s, while five ductility factors, i.e., $\mu = 2$, 3, 4, 5, and 6, were chosen deliberately to consider various levels of inelasticity that the structural systems are anticipated to experience during the earthquake-induced strong ground motions. Three damping ratios, i.e., $\xi = 0.02$, 0.05, and 0.10, and five postyield stiffness ratios, i.e., $\alpha = -0.10$, -0.05, 0.00, 0.05, and 0.10, are, respectively, adopted. In addition, the elastic-perfectly plastic (EPP) model was chosen herein.

In this study, the influence of the P-delta effect on YPS is also considered. Figure 2 shows the force-displacement relationship considering P-delta effects. In this system, the lateral stiffness can be written as follows [29]:

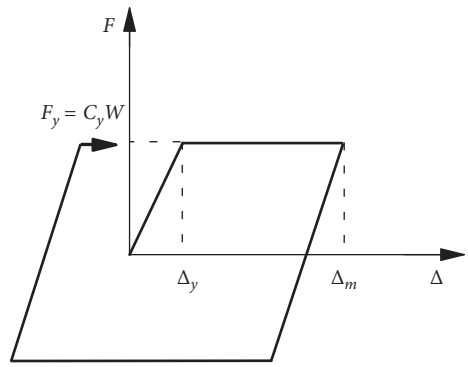

Figure 1: Force-deformation law of an EPP model.

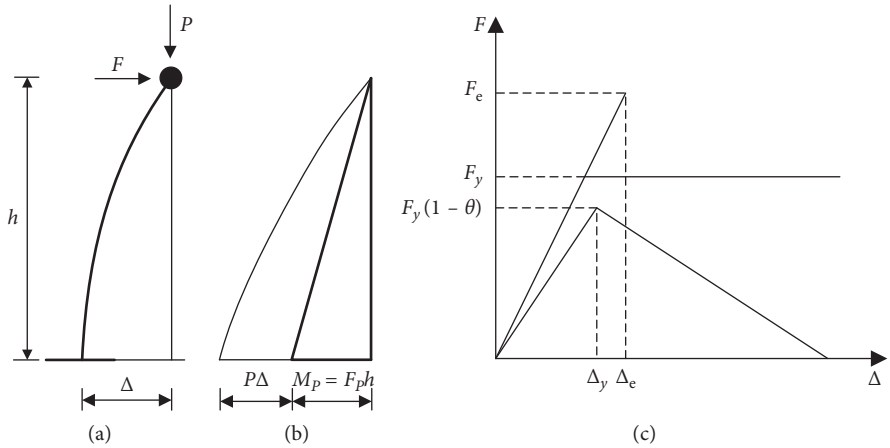

Figure 2: Force-displacement relationships considering P-delta effects.

$$k = k_0(1-\theta),$$
$$\theta = \frac{P}{k_0 h}, \tag{3}$$

where k is the lateral stiffness, k_0 is the lateral stiffness of systems without P-delta effects, θ is the stability coefficient, and P is the gravity force. Note that F, M_P, F_P, F_e, and Δ_e are the lateral force, moment of systems without P-delta effects, lateral force of systems without P-delta effects, maximum elastic force, and maximum elastic displacement, respectively. The P-delta effect on YPS is considered through changing the values of θ, say 0.05 and 0.10. The yield displacement for SDOF systems with P-delta effects can be calculated as follows:

$$\Delta_y = \frac{M_y}{k_0 h}, \tag{4}$$

where M_y is the yield moment.

The procedures for computation of the YPS can be divided into four steps: (1) determination of a ground motion and structural parameters, i.e., vibration period, mass, damping ratio, etc.; (2) iterative calculations until a specified ductility factor is achieved; (3) calculation of C_y and Δ_y; and (4) repetition of the above procedures for different ground motions or structural parameters. Figure 3 illustrates the flowchart for the computation of YPS.

3. Ground Motions

This study selects 601 strong ground motions from 16 major global earthquakes, as shown in Table 1. The selected ground motions can be divided into four groups based on shear wave velocity V_{S30}, and the details can be found in Table 2. Note that all the ground motions were downloaded from the PEER ground motion database [31] and the China Earthquake Networks Center [32]. The criteria for selecting ground motions can be summed up as follows: (1) The recording stations contain sufficient information (i.e., geological-geotechnical). (2) The moment magnitude is higher than or equal to 6.0. (3) For soil sites B, C, and D, the ground motions were recorded on the accelerographic stations, the free stations, and the first-floor low-rise buildings. (4) For soil site E, the ground motions were recorded on the free stations because the soil-structure interaction (SSI) effects cannot be ignored for the low-rise buildings located in the soft soil site.

4. Yield Point Spectra

4.1. Mean YPS. In this section, in order to normalize the YPS, ground motions were scaled to 0.1 g. A total amount of 432,720 YPS indices are computed for 601 earthquake ground motions, 120 vibration periods, and 6 levels of ductility factors. Note that Δ_y ($\mu = 1$) is the maximum elastic displacement.

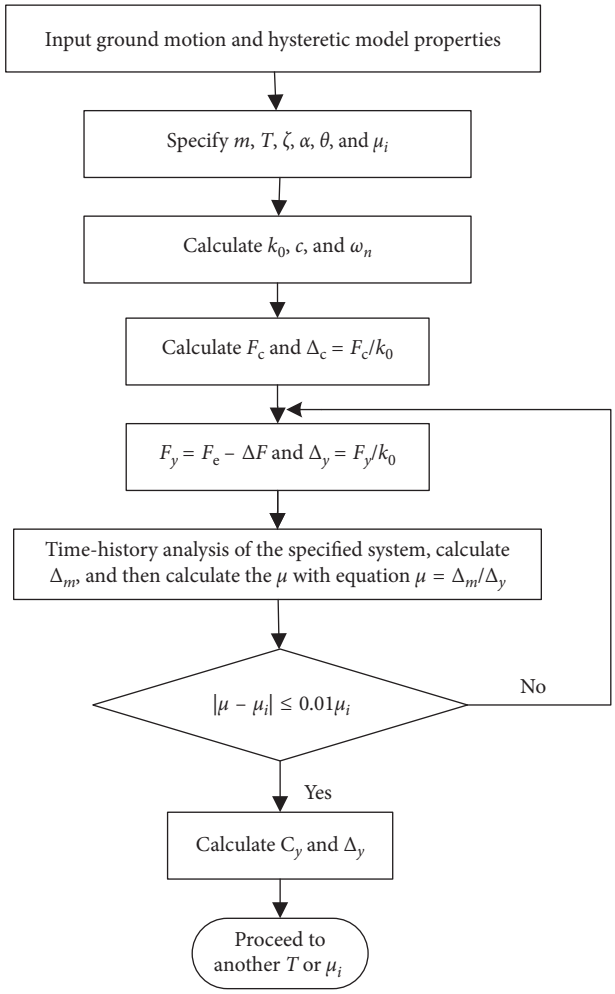

Figure 3: Flowchart for computation of YPS.

Figure 4 shows the mean YPS for four different site classes. It can be observed from Figure 4 that, for a given ductility factor, Δ_y increases with the increase of vibration periods, while C_y increases initially and then decreases when vibration periods increase. The yield displacement Δ_y is close to 0 when vibration periods are close to 0 as the stiffness of a structure (T close to 0) tends towards infinity.

On the contrary, Δ_y multiplied by μ is close to the maximum elastic displacement, Δ_y ($\mu = 1$), because of the equal displacement rule. Over the whole period range, YPS are highly dependent on vibration periods. For a given vibration period, C_y and Δ_y decrease with the increase of the ductility factor, while no obvious changes in YPS's shape can be observed. For different site classes, the tendency of YPS is maintained consistently; for example, the varying rules of C_y and Δ_y with the increase of vibration periods and ductility factor are the same. However, for some specific characteristics, i.e., the location of the maximum point, YPS for firm soil sites (e.g., sites B, C, and D) are obviously different from those for soft soil sites (e.g., site E). For example, the maximum point of YPS for firm soil sites corresponds to a vibration period of 0.3 s, while that for a soft soil site corresponds to a vibration period of 0.7 s. It is because ground motions recorded at firm soil sites are characterized by broadband high-frequency content features, while those recorded at soft soil sites are characterized by narrowband low-frequency content features [33]. This is also corroborated by many past investigations [34–36] that spectral amplifications are much higher for softer soil sites, particularly in the medium- to long-period range. Similar findings were observed by additional studies [37, 38].

In order to study the effects of soil type on YPS more clearly, Figure 5 presents YPS for four soil sites with two ductility factors. It can be observed from Figure 5 that, for a given vibration period and ductility factor, C_y and Δ_y increase when the soil tends to soften. The tendency will become weaker with an increasing ductility factor, but it still has a difference in YPS among different soil sites. Thus, YPS for different soil sites need to receive special attention.

4.2. Dispersion of YPS. In statistical studies, mean spectra are very important because they can reflect the average tendency of the sample, while it is equally important to know the scatter of the sample, e.g., dispersion. In this study, the dispersion is qualified by the coefficient of variation (COV). It should be noted that, for a given vibration period, the ratio of C_y to Δ_y is constant for structures under different ground motions (see equation (1)) even though the values of C_y and Δ_y are not the same. This means that the COVs of C_y and Δ_y are the same even though the mean and standard deviation values of C_y and Δ_y are different. Thus, the dispersion of YPS is investigated by analyzing the dispersion of C_y.

Figure 6 shows the COVs of C_y for four soil sites considering various combinations of T and μ. Previous investigations [39, 40] pointed out that relatively large COVs would be produced in the long-period range when using the acceleration parameter to normalize response spectra, while, as expected, the COVs increase with the increase of vibration periods. For example, for a given ductility factor $\mu = 3$, the COVs increase from 30% at $T = 0.5$ s to 60% at $T = 4.5$ s, as shown in Figure 6(a). At the same time, the ductility factor has a minor effect on the COVs of C_y, and increasing the ductility factor will lead to a slight increase of COVs except for $\mu = 1$. For a vibration period larger than 2.0 s, the COVs can reach 50%, meaning that the randomness of the earthquake ground motion may have a greater impact on the COVs of C_y for long-period structures. Over the whole period range, COVs are within 80%.

4.3. Effects of Damping Ratio. Structures under earthquake excitation begin to vibrate and tend to cease vibration because of the effect of damping. The damping effect on the structural response cannot be ignored and received a lot of attention [41, 42]. Thus, it is very important to study the effects of damping on YPS through three damping ratios (i.e., $\xi = 0.02$, 0.05, and 0.10) selected herein. Figure 7 presents YPS for soil site B considering three damping ratios and two ductility factors. It can be seen that C_y and Δ_y decrease with the increase of damping ratios. The latter is because the energy, dissipated by damping, increases with an increasing damping ratio, which will cause a reduction of the

Table 1: Selected ground motions in this study.

Earthquake name	Time	Moment magnitude, M_w	Number of ground motions
Cape Mendocino	1992	7.1	10
Chi-Chi	1999	7.6	91
Coalinga	1983	6.5	14
Duzce	1999	7.3	33
Imperial Valley	1979	6.9	35
Kern County	1952	7.7	10
Kobe	1995	7.2	11
Kocaeli	1999	7.8	39
Landers	1992	7.4	63
Loma Prieta	1989	7.1	58
Morgan Hill	1984	6.1	34
Northridge	1986	6.7	63
Palm Springs	1986	6.0	22
San Fernando	1971	6.6	25
Wenchuan	2008	8.0	88
Lijiang	1996	7.0	5

Table 2: Site classifications defined in NEHRP [30].

Soil type	Shear wave velocity, V_{S30} (m/s)	Number of ground motions
B	760–1500	192
C	360–760	173
D	180–360	173
E	<180	73

energy dissipated by yielding or inelastic deformation [43]. These phenomena can also be found in other inelastic indices such as the strength reduction factor [44] and hysteretic energy [45]. The difference in YPS caused by the damping ratio will reduce for weaker structures, i.e., structures with $\mu = 5$.

In order to quantify the effects of damping ratios on YPS, the ratio of Δ_y with $\xi = 0.02$ and 0.10 normalized by Δ_y with $\xi = 0.05$ versus T is plotted for soil site B, as shown in Figure 8. It can be observed from Figure 8 that the effects of damping ratios are more profound for Δ_y (i.e., $\mu = 1$). This is because the total energy of the elastic systems consists of elastic energy and damping energy, and thus, the elastic displacement is sensitive to the change of damping ratios. At the same time, the total energy of an inelastic system consists of inelastic energy, elastic energy, and damping energy, and thus, damping has a moderate effect on the yield displacement Δ_y of inelastic systems. In the short-period range (0–0.5 s), as shown in Figure 8(a), the normalized Δ_y increases with the increase of vibration periods, while it slightly changes with the increase of vibration periods in the medium- to long-period range. Over the whole period range, the effects of damping ratios on the Δ_y are within 40% for elastic systems, while they are within 20% for inelastic systems.

4.4. Effects of Postyield Stiffness. This section selects four postyield stiffness ratios to investigate the effect of postyield stiffness on YPS, including two positive postyield stiffness ratios, 0.05 and 0.10, and two negative postyield stiffness ratios, −0.05 and −0.10. Figure 9 illustrates YPS for soil site B considering five postyield stiffness ratios and two ductility factors. It can be observed from Figure 9 that C_y and Δ_y increase with the decrease of postyield stiffness ratios, which is more pronounced for weaker structures ($\mu = 5$).

To quantitatively study the effects of postyield stiffness ratios on YPS, Δ_y for selected postyield stiffness ratios, −0.05, −0.10, 0.05, and 0.10, and soil site B is normalized by Δ_y ($\alpha = 0$), as shown in Figure 10. The difference of the normalized Δ_y caused by postyield stiffness ratios is more pronounced for weaker structures (i.e., with $\mu > 4$). For $\alpha < 0$, the normalized Δ_y increases with the increase of vibration periods in the short-period range, while it fluctuates with the change of vibration periods in the medium- to long-period range. For $\alpha > 0$, the normalized Δ_y decreases with the increase of vibration periods in the short-period range, while it remains almost constant with the change of vibration periods in the medium- to long-period range. The normalized Δ_y is within [80%, 100%] for $\alpha > 0$, while it is within [100%, 200%] for $\alpha < 0$. Structures with negative postyield stiffness ratios subjected to earthquake excitation may produce a Δ_y twice as big as Δ_y at $\alpha = 0$. At the same time, Δ_y at $\alpha > 0$ may be equal to 80% of Δ_y at $\alpha = 0$ when subjected to the same earthquake excitation. This means that compared with a zero postyield stiffness ratio, a positive postyield stiffness ratio is beneficial to structural inelastic responses, while the negative postyield stiffness ratio is harmful to structural inelastic responses.

4.5. Effects of the P-Delta Effect. Past studies reported that P-delta effects can exert a significant effect on structural inelastic responses, especially for multistory moment-resistant frames [46–48]. Thus, it is necessary to investigate the P-delta effects on YPS. Figure 11 presents YPS for soil site B considering three values of θ (i.e., 0.00, 0.05, and 0.10) and two ductility factors. As can be seen from Figure 11, C_y and Δ_y will be greater when the θ increases for weaker structures

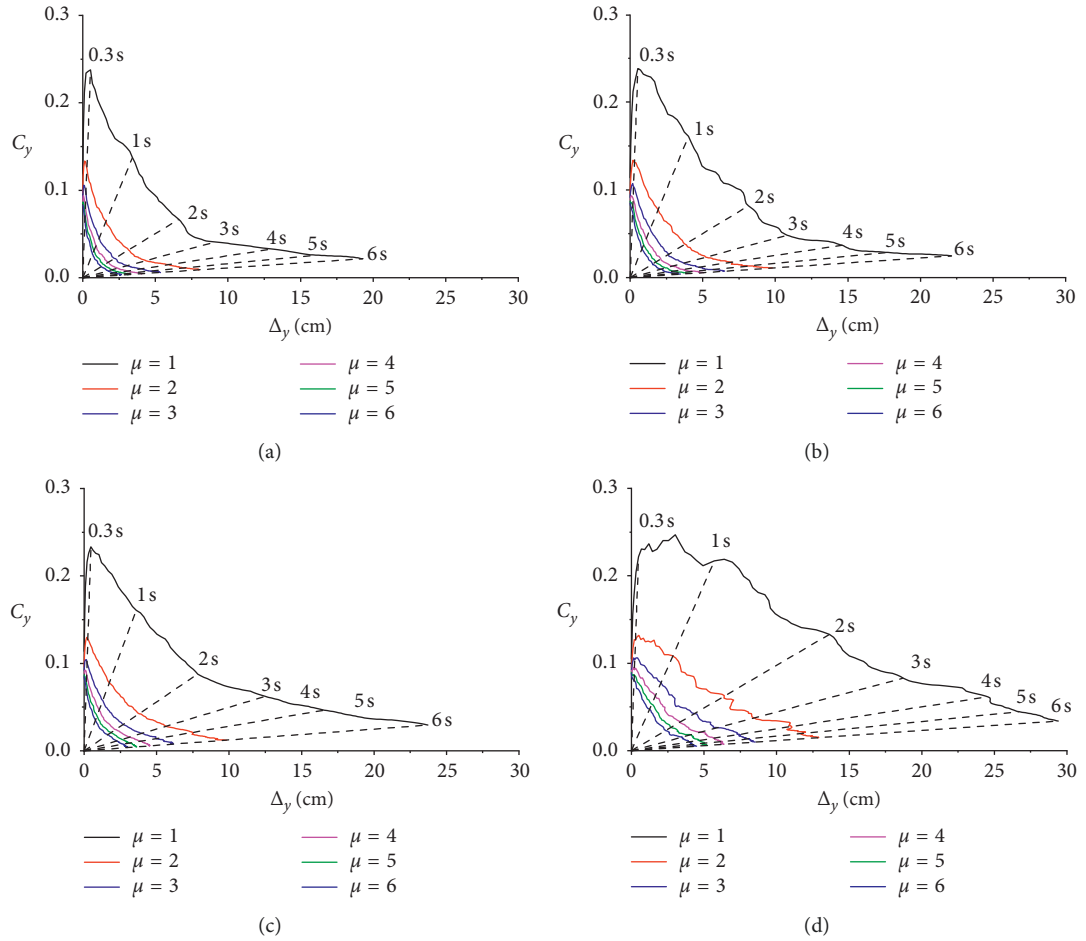

Figure 4: YPS for six-SDOF systems on four different site classes: (a) site B; (b) site C; (c) site D; (d) site E.

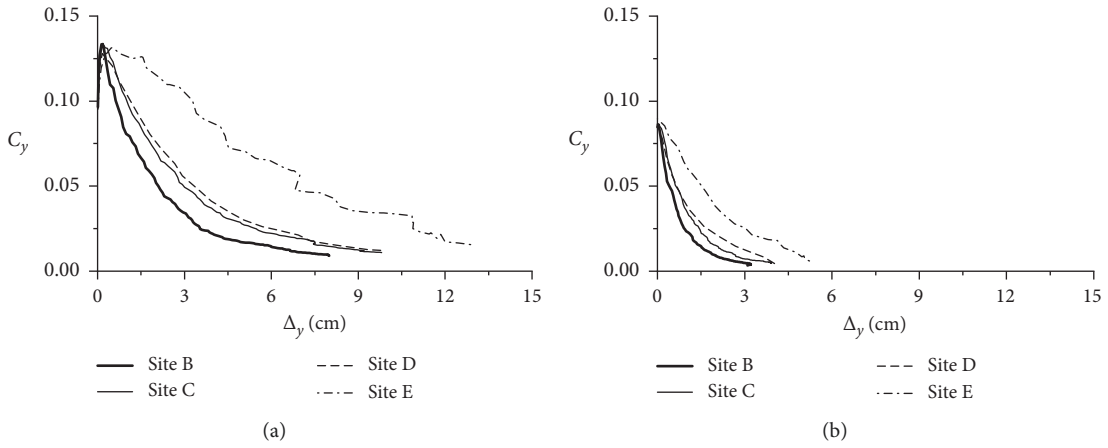

Figure 5: Effects of the soil site on YPS considering two ductility factors: (a) $\mu = 2$; (b) $\mu = 5$.

(i.e., with $\mu = 5$), while the θ has a negligible effect on YPS for stronger structures (i.e., with $\mu = 2$). To quantitatively investigate the P-delta effect on the Δ_y, the Δ_y with two values of θ (i.e., 0.05 and 0.10) is normalized by Δ_y without P-delta effects for soil site B by considering six ductility factors, as shown in Figure 12. It can be observed from Figure 12 that the normalized Δ_y increases with an increasing ductility factor while the value of normalized Δ_y is slightly larger than 1. The latter means that the P-delta effect can be ignored for elastic systems. In the short-period range, the normalized Δ_y increases with the increase of vibration periods, and it fluctuates with the change of vibration periods in the

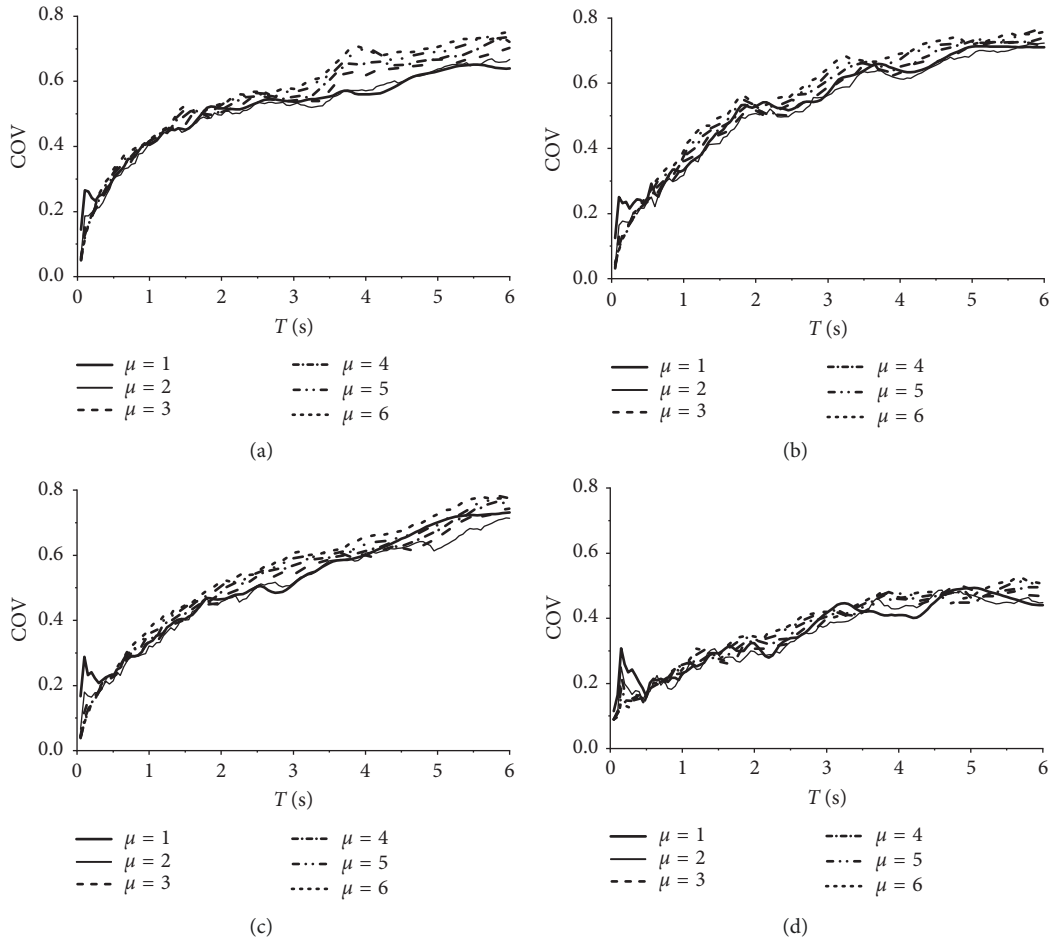

Figure 6: COV versus considering various combinations of μ and T on four different site classes: (a) site B; (b) site C; (c) site D; (d) site E.

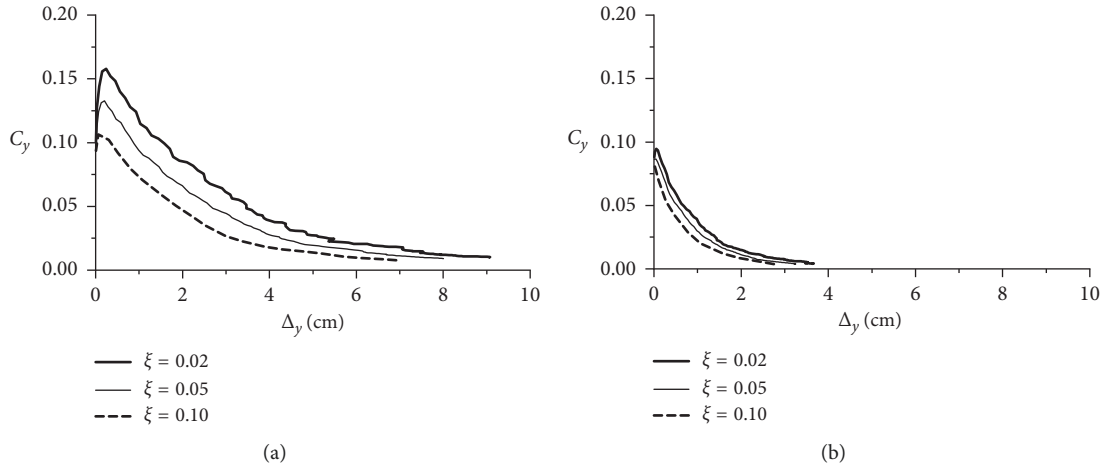

Figure 7: Effects of damping ratios on YPS for soil site B considering two ductility factors: (a) $\mu = 2$; (b) $\mu = 5$.

medium- to long-period range. The difference of Δ_y caused by the ductility factor remains constant with varying vibration periods. Over the whole period range, the normalized Δ_y is within [100%, 160%], and it becomes significantly larger for $\theta = 0.10$, reaching 220%.

5. Prediction Equation

The prediction equation of YPS is useful to help engineers to adopt YPS-based seismic design in performance-based earthquake engineering (PBEE), and thus, a prediction

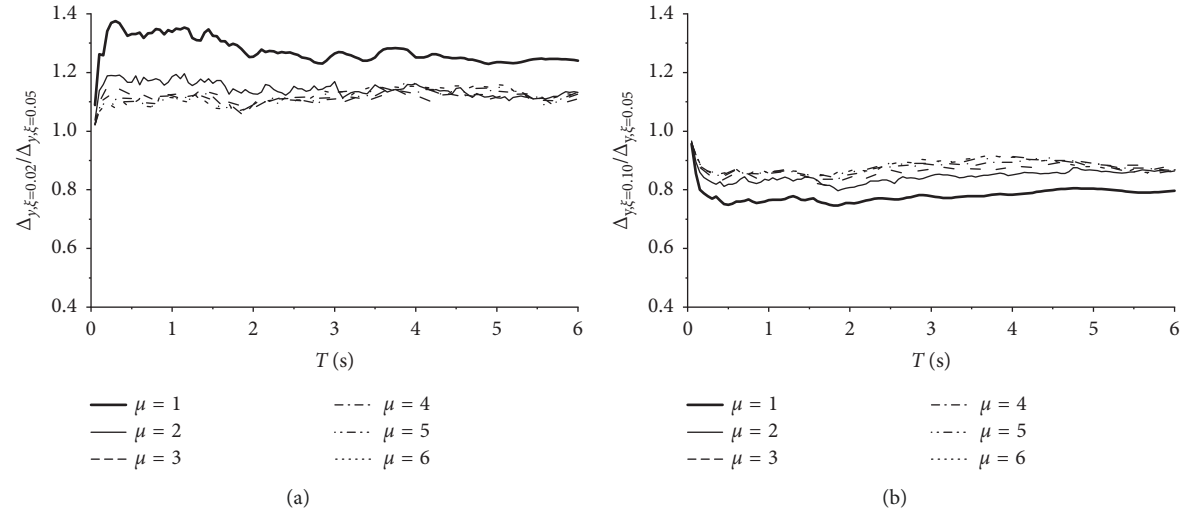

Figure 8: Normalized Δ_y for two damping ratios and soil site B considering various combinations of T and μ: (a) $\xi = 0.02$; (b) $\xi = 0.10$.

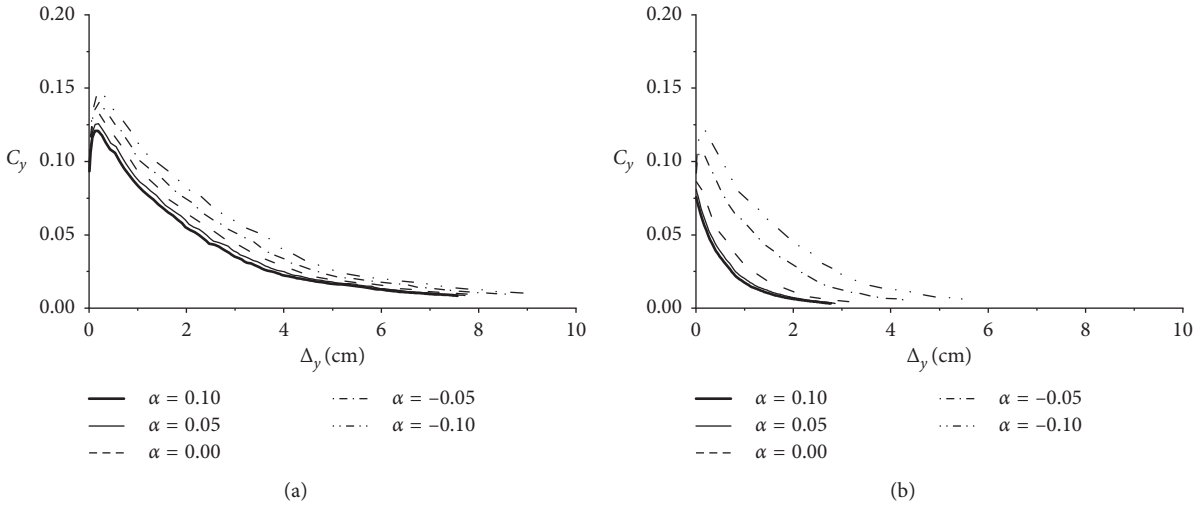

Figure 9: Effects of postyield stiffness on YPS for soil site B considering two ductility factors: (a) $\mu = 2$; (b) $\mu = 5$.

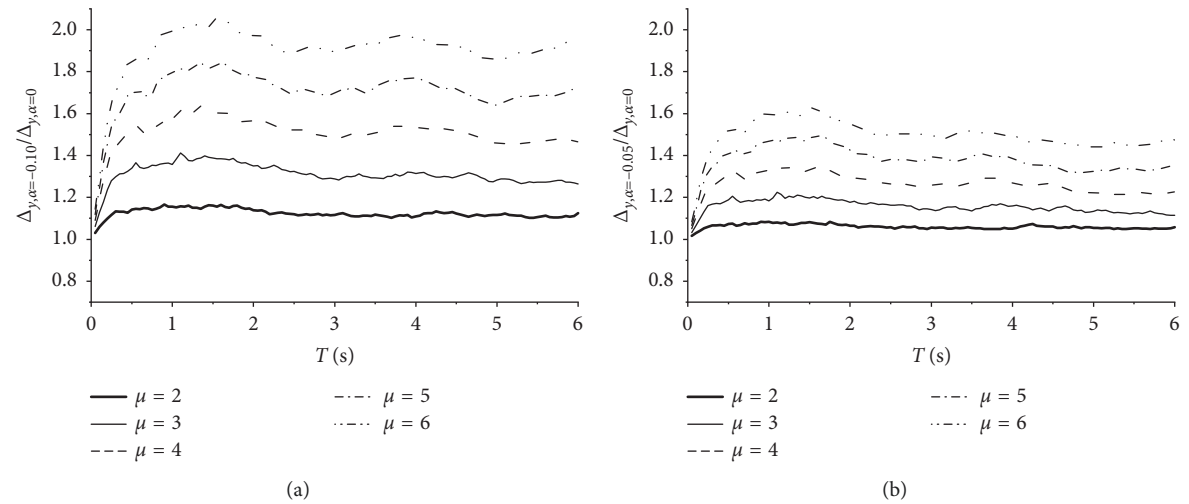

Figure 10: Continued.

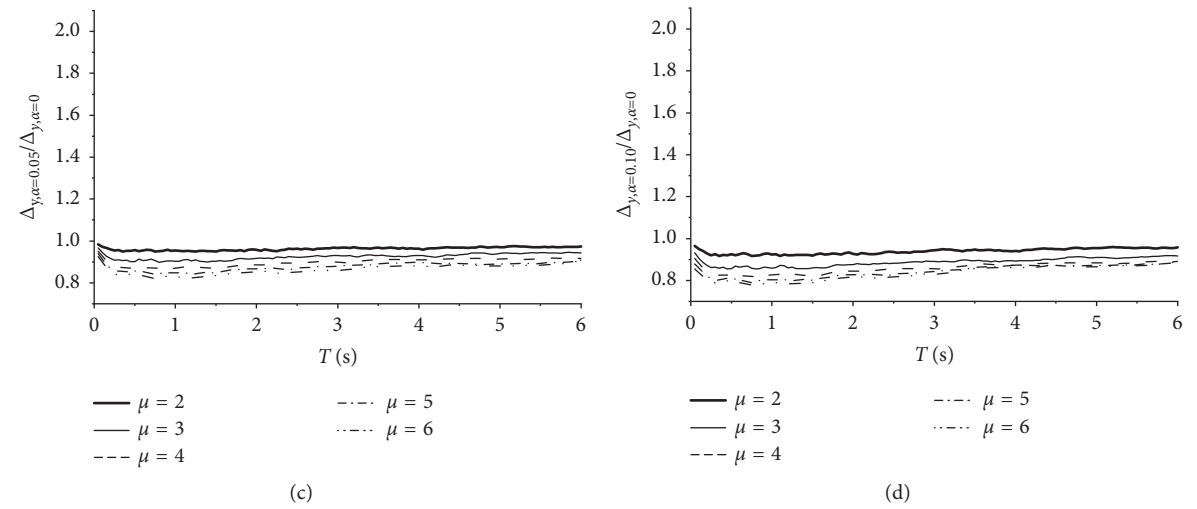

Figure 10: Normalized Δ_y for four postyield stiffness ratios and soil site B considering various combinations of T and μ: (a) $\alpha = -0.10$; (b) $\alpha = -0.05$; (c) $\alpha = 0.05$; (d) $\alpha = 0.10$.

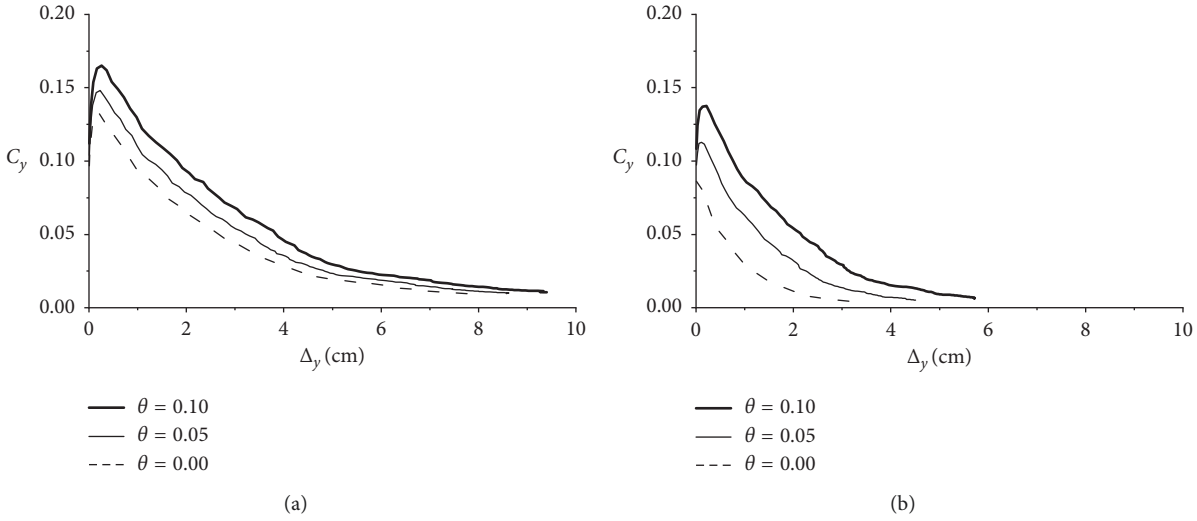

Figure 11: Effects of θ on YPS for soil site B considering two ductility factors: (a) $\mu = 2$; (b) $\mu = 5$.

equation is given based on the statistical results in this section. The analytical expression is provided as follows:

$$C_y = \begin{cases} a\Delta_y + b, & \Delta_y \le \Delta_1, \\ C_{y,\Delta_1} + \dfrac{\Delta_y - \Delta_1}{\Delta_2 - \Delta_1}\left(C_{y,\Delta_2} - C_{y,\Delta_1}\right), & \Delta_1 < \Delta_y < \Delta_2, \\ c\exp\left(d\Delta_y\right) + e, & \Delta_y \ge \Delta_2, \end{cases} \tag{5}$$

where C_y is the yield strength coefficient and Δ_y is the yield displacement. In this study, equation (5) was calculated by using the nonlinear least-squares regression analysis that can be implemented by many computational methods, such as Gauss–Newton and steepest descent algorithms. Though the two algorithms have been shown to be very effective in dealing with nonlinear least-squares problems, they have several serious drawbacks (e.g., divergence problems and slow progressive convergence problems). To avoid the problems, the Levenberg–Marquardt algorithm [49, 50] was designed, which is a combination of the Gauss–Newton and steepest descent algorithms. It is an iterative technique for obtaining the minimum value of the sum of square errors, as follows:

$$E = \frac{1}{2}\sum k\left(e_k\right)^2 = \frac{1}{2}\|e\|^2, \tag{6}$$

where E is the sum of square errors, e_k is the error for the kth exemplar or pattern, and e is the vector for the element e_k. Hence, parameters Δ_1, Δ_2, a, b, c, d, and e in equation (5)

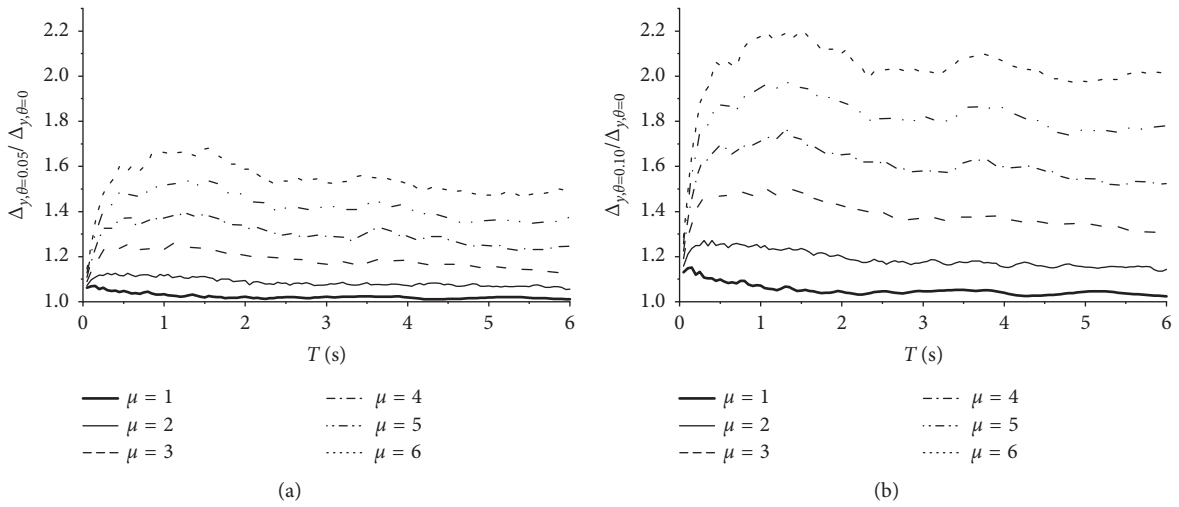

Figure 12: Normalized Δ_y for four postyield stiffness ratios and soil site B considering various combinations of T and μ: (a) $\theta = 0.05$; (b) $\theta = 0.10$.

Table 3: Parameters in equation (5).

Site class	μ	a	b	c	d	e	Δ_1	Δ_2
B	1	0.588	0.141	0.551	−0.287	0.021	0.233	0.532
	2	0.328	0.116	0.131	−0.632	0.009	0.133	0.278
	3	0.222	0.109	0.104	−0.965	0.006	0.105	0.216
	4	0.140	0.105	0.091	−1.267	0.004	0.090	0.183
	5	0.037	0.102	0.082	−1.569	0.004	0.082	0.163
	6	−0.023	0.100	0.076	−1.856	0.003	0.075	0.148
C	1	0.174	0.130	0.267	−0.074	0.013	0.210	0.531
	2	0.098	0.100	0.146	−0.179	0.008	0.127	0.293
	3	0.050	0.093	0.116	−0.284	0.006	0.104	0.233
	4	0.020	0.089	0.101	−0.376	0.004	0.092	0.202
	5	−0.005	0.086	0.092	−0.466	0.004	0.084	0.182
	6	−0.024	0.084	0.085	−0.548	0.003	0.079	0.167
D	1	0.191	0.133	0.229	−0.069	0.027	0.193	0.470
	2	0.099	0.101	0.129	−0.155	0.010	0.113	0.256
	3	0.049	0.094	0.103	−0.241	0.006	0.093	0.201
	4	0.017	0.089	0.090	−0.313	0.004	0.082	0.174
	5	−0.011	0.086	0.081	−0.370	0.003	0.075	0.156
	6	−0.033	0.084	0.075	−0.435	0.002	0.070	0.143
E	1	0.103	0.112	0.333	−0.024	−0.033	0.478	3.025
	2	0.050	0.096	0.171	−0.062	−0.013	0.277	1.553
	3	0.023	0.092	0.129	−0.097	−0.008	0.230	1.130
	4	0.006	0.090	0.111	−0.141	−0.005	0.206	0.942
	5	−0.007	0.088	0.099	−0.184	−0.004	0.190	0.832
	6	−0.017	0.087	0.091	−0.223	−0.004	0.179	0.738
All sites	1	0.178	0.137	0.263	−0.082	0.009	0.225	0.532
	2	0.096	0.103	0.142	−0.193	0.004	0.130	0.286
	3	0.047	0.095	0.112	−0.304	0.003	0.105	0.223
	4	0.014	0.090	0.097	−0.407	0.003	0.092	0.191
	5	−0.012	0.087	0.088	−0.511	0.002	0.083	0.171
	6	−0.033	0.084	0.082	−0.605	0.001	0.078	0.156

were evaluated by the Levenberg–Marquardt algorithm until the minimal error was achieved between analytical and predicted values. The above parameters are listed in Table 3 for various soil sites and ductility factors.

Note that the above equation of YPS is only suitable for earthquake ground motions with a peak ground acceleration (PGA) of 0.1 g, and thus, it is necessary to extend the equation so that it can be suitable for earthquake ground

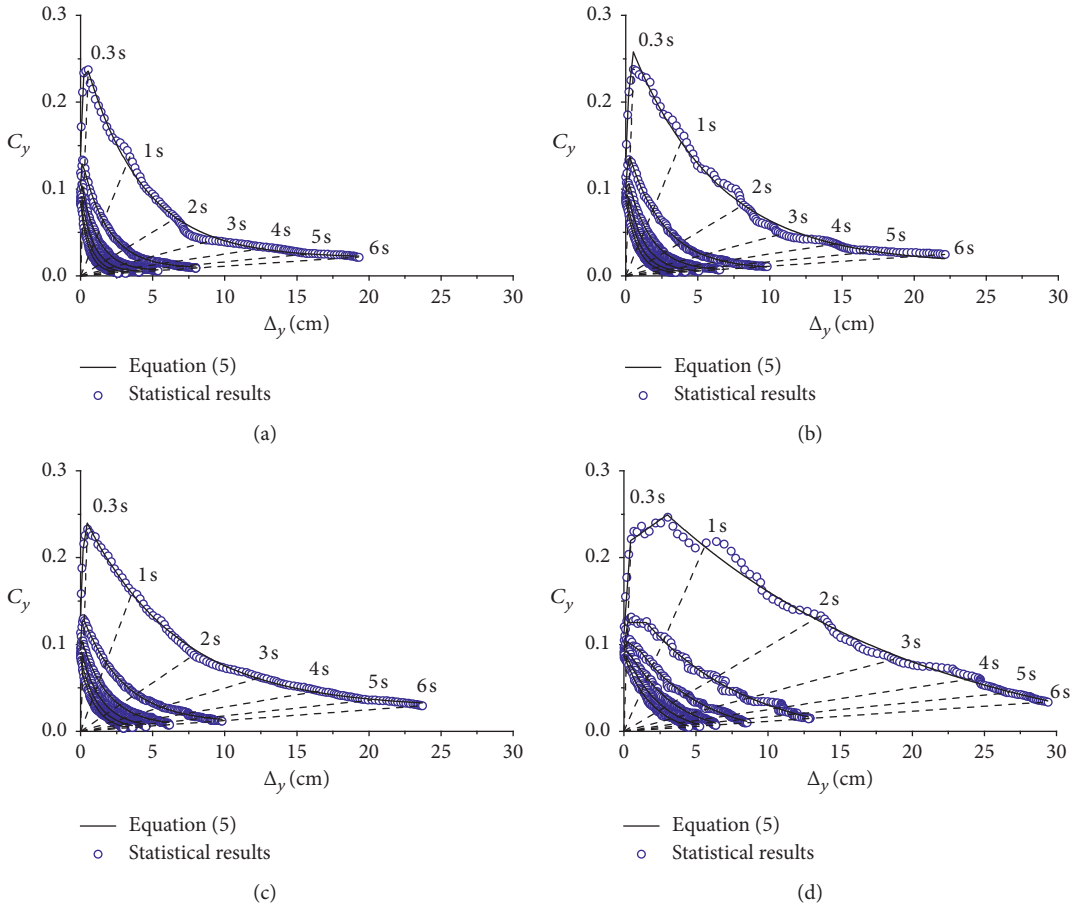

Figure 13: Comparisons of the results predicted by equation (5) and the analytical results considering four soil sites: (a) site B; (b) site C; (c) site D; (d) site E.

motions with any arbitrary value of PGA. The equation is given as follows:

$$C_y = \frac{\text{PGA}}{0.1} \cdot f\left(\frac{0.1}{\text{PGA}}\Delta_y\right), \tag{7}$$

where PGA is the peak ground acceleration (g) and $f(\cdot)$ represents equation (5).

In order to demonstrate the fitting precision of the proposed equation, the results obtained using equation (5) and the statistical analysis are plotted in Figure 13. It can be seen that the predicted results agree well with the analytical results, meaning that the predicted equation can provide results with a high degree of precision.

6. Conclusions

This study systematically investigated YPS. A total of 601 ground motions from global earthquakes were selected and divided into four groups based on NEHRP. A prediction equation was proposed based on the statistical results in which the effects of damping ratios and P-delta effects were considered. The main conclusions can be drawn as follows:

(1) YPS are highly dependent on vibration periods. For example, the yield displacement, Δ_y, increases with the increase of vibration periods. The same tendency can be observed for the yield strength coefficient, C_y, in the short-period range, while the reverse phenomenon is presented in the medium- to long-period range. YPS are also affected by the ductility factor and decrease with the increase of the ductility factor. Besides, the soil site also has a significant effect on YPS, especially for soft soils.

(2) The dispersion of C_y/Δ_y is studied by calculating the COV. The COV depends on vibration periods and increases with the increase of vibration periods. Over the whole period range, the COV is less than 80%. The difference in the COV caused by the ductility factor is not obvious.

(3) The damping ratio has a moderate effect on YPS. For inelastic systems, Δ_y increases between 10% and 18% when decreasing damping ratios from 0.05 to 0.02, while Δ_y decreases between 10% and 20% when increasing damping ratios from 0.05 to 0.10. However, for elastic systems, Δ_y increases or decreases may be amplified 1.5 times those for inelastic systems.

(4) YPS increase with the decrease of the postyield stiffness, and this decrease is more pronounced for

weaker structures (i.e., with $\mu = 5$). Δ_y decreases between 10% and 20% for structures that have positive postyield stiffness ratios, while Δ_y increases between 10% and 200% for structures that have negative postyield stiffness ratios. Thus, the positive postyield stiffness ratio is beneficial for structural dynamic responses.

(5) YPS increase with the increase of the stability coefficient, θ, especially for weaker structures. The structures with inelastic deformations are sensitive to P-delta effects because the P-delta effects have a slight influence on elastic structures. The Δ_y increases caused by P-delta effects are between 10% and 120%.

(6) A prediction equation for YPS was proposed including six parameters that were determined by soil site classes and ductility factors. The equation can be used to predict YPS with high precision because the results predicted by the equation agree well with analytical results.

Note that this study focused on YPS for an EPP model in which the stiffness degradation and strength deterioration are not considered. Thus, the effect of hysteretic models on YPS deserves further study.

Data Availability

The ground motions used in this study are deposited in the Pacific Earthquake Engineering Research Centre (PEER) Next Generation Attenuation (NGA) Relationships database (http://ngawest2.berkeley.edu/) and the China Earthquake Networks Center.

Conflicts of Interest

The authors declare that there are no conflicts of interest regarding the publication of this paper.

Acknowledgments

This investigation was supported by the National Natural Science Foundation of China (Nos. 51825801 and 51708161), the China Postdoctoral Science Foundation (Nos. 2018M641834, 2018T110305, and 2019T120272), and the Fundamental Research Funds for the Central Universities (Grant No. HIT. NSRIF. 2020085). These supports are greatly appreciated.

References

[1] N. Augenti and F. Parisi, "Learning from construction failures due to the 2009 L'Aquila, Italy, earthquake," *Journal of Performance of Constructed Facilities*, vol. 24, no. 6, pp. 536–555, 2010.

[2] B. Zhao, F. Taucer, and T. Rossetto, "Field investigation on the performance of building structures during the 12 May 2008 Wenchuan earthquake in China," *Engineering Structures*, vol. 31, no. 8, pp. 1707–1723, 2009.

[3] M. J. N. Priestley, "Performance based seismic design," in *Proceedings of the 12th WCEE*, pp. 1–22, Auckland, New Zeland, January 2000.

[4] M. S. Medhekar and D. J. L. Kennedy, "Displacement-based seismic design of buildings-theory," *Engineering Structures*, vol. 22, no. 3, pp. 201–209, 2000.

[5] M. J. N. Priestley, G. M. Calvi, and M. J. Kowalsky, *Displacement-Based Seismic Design of Structures*, IUSS Press, Pavia, Italy, 2007.

[6] K. Muto, R. Takahasi, I. Aida et al., "Nonlinear response analyzers and application to earthquake resistant design," in *Proceedings of the Second World Conference on Earthquake Engineering*, pp. 649–668, Tokyo, Japan, July 1960.

[7] A. S. Veletsos and N. M. Newmark, "Effect of inelastic behavior on the response of simple systems to earthquake motions," in *Proceedings of the Second World Conference on Earthquake Engineering*, pp. 895–912, Tokyo, Japan, July 1960.

[8] J. P. Moehle, "Strong motion drift estimates for R/C structures," *Journal of Structural Engineering*, vol. 110, no. 9, pp. 1988–2001, 1984.

[9] J. P. Moehle, "Displacement-based design of RC structures subjected to earthquakes," *Earthquake Spectra*, vol. 8, no. 3, pp. 403–428, 1992.

[10] G. M. Calvi and G. R. Kingsley, "Displacement-based seismic design of multi-degree-of-freedom bridge structures," *Earthquake Engineering and Structural Dynamics*, vol. 24, no. 9, pp. 1247–1266, 1995.

[11] M. J. Kowalsky, M. J. N. Priestley, and G. A. MacRae, "Displacement-based design of RC bridge columns in seismic regions," *Earthquake Engineering and Structural Dynamics*, vol. 24, no. 12, pp. 1623–1643, 1995.

[12] M. J. N. Priestley, "Displacement-based seismic assessment of reinforced concrete buildings," *Journal of Earthquake Engineering*, vol. 1, no. 1, pp. 157–192, 1997.

[13] M. J. N. Priestley and G. M. Calvi, "Towards a capacity-design assessment procedure for reinforced concrete frames," *Earthquake Spectra*, vol. 7, no. 3, pp. 413–437, 1991.

[14] E. I. Katsanos and A. G. Sextos, "Structure-specific selection of earthquake ground motions for the reliable design and assessment of structures," *Bulletin of Earthquake Engineering*, vol. 16, no. 2, pp. 583–611, 2018.

[15] F. Mazza, M. Mazza, and A. Vulcano, "Displacement-based seismic design of hysteretic damped braces for retrofitting in-elevation irregular r.c. framed structures," *Soil Dynamics and Earthquake Engineering*, vol. 69, pp. 115–124, 2015.

[16] M. Aschheim and E. F. Black, "Yield point spectra for seismic design and rehabilitation," *Earthquake Spectra*, vol. 16, no. 2, pp. 317–336, 2000.

[17] M. Aschheim, "Seismic design based on the yield displacement," *Earthquake Spectra*, vol. 18, no. 4, pp. 581–600, 2002.

[18] T. N. Tjhin, M. A. Aschheim, and J. W. Wallace, "Yield displacement-based seismic design of RC wall buildings," *Engineering Structures*, vol. 29, no. 11, pp. 2946–2959, 2007.

[19] A. Tsiavos and B. Stojadinović, "Constant yield displacement procedure for seismic evaluation of existing structures," *Bulletin of Earthquake Engineering*, vol. 17, no. 4, pp. 2137–2164, 2019.

[20] E. Hernández-Montes and M. Aschheim, "An estimate of the yield displacement of coupled walls for seismic design," *International Journal of Concrete Structures and Materials*, vol. 11, no. 2, pp. 275–284, 2017.

[21] E. Hernández-Montes and M. A. Aschheim, "A seismic design procedure for moment-frame structures," *Journal of Earthquake Engineering*, pp. 1–20, 2017.

[22] M. Aschheim and E. H. Montes, "The representation of P-Δ effects using yield point spectra," *Engineering Structures*, vol. 25, no. 11, pp. 1387–1396, 2003.

[23] Y. Bozorgnia, M. M. Hachem, and K. W. Campbell, "Deterministic and probabilistic predictions of yield strength and inelastic displacement spectra," *Earthquake Spectra*, vol. 26, no. 1, pp. 25–40, 2010.

[24] E. I. Katsanos and D. Vamvatsikos, "Yield frequency spectra and seismic design of code-compatible RC structures: an illustrative example," *Earthquake Engineering and Structural Dynamics*, vol. 46, no. 11, pp. 1727–1745, 2017.

[25] D. Vamvatsikos and M. A. Aschheim, "Performance-based seismic design via yield frequency spectra," *Earthquake Engineering and Structural Dynamics*, vol. 45, no. 11, pp. 1759–1778, 2016.

[26] American Society of Civil Engineers, *ASCE7-10, Minimum Design Loads for Buildings and Other Structures*, American Society of Civil Engineers, Reston, VA, USA, 2013.

[27] CEN, *Eurocode 8: Design of Structures for Earthquake Resistance. Part 1: General Rules, Seismic Actions and Rules for Buildings*, CEN, Brussels, Belgium, 2004.

[28] FEMAP-750, *NEHRP Recommended Seismic Provisions for New Buildings and Other Structures*, FEMAP, Washington, DC, USA, 2009.

[29] D. Bernal, "Amplification factors for inelastic dynamicp-Δ effects in earthquake analysis," *Earthquake Engineering and Structural Dynamics*, vol. 15, no. 5, pp. 635–651, 1987.

[30] FEMA-450, *NEHRP Recommended Provisions for Seismic Regulations for New Buildings and Other Structures*, BSSC, Washington, DC, USA, 2003.

[31] PEER, 2016, http://ngawest2.berkeley.edu/.

[32] CENC, "China earthquake networks center," 2016.

[33] J. Ruiz-García and H. Guerrero, "Estimation of residual displacement ratios for simple structures built on soft-soil sites," *Soil Dynamics and Earthquake Engineering*, vol. 100, pp. 555–558, 2017.

[34] E. Kalkan and P. Gu¨lkan, "Site-dependent spectra derived from ground motion records in Turkey," *Earthquake Spectra*, vol. 20, no. 4, pp. 1111–1138, 2004.

[35] R. D. Borcherdt, "Estimates of site-dependent response spectra for design (methodology and justification)," *Earthquake Spectra*, vol. 10, no. 4, pp. 617–653, 1994.

[36] D. M. Boore, J. P. Stewart, E. Seyhan, and G. M. Atkinson, "NGA-west2 equations for predicting PGA, PGV, and 5% damped PSA for shallow crustal earthquakes," *Earthquake Spectra*, vol. 30, no. 3, pp. 1057–1085, 2014.

[37] E. Miranda and J. Ruiz-Garcia, "Influence of stiffness degradation on strength demands of structures built on soft soil sites," *Engineering Structures*, vol. 24, no. 10, pp. 1271–1281, 2002.

[38] P. Panyakapo, "Evaluation of site-dependent constant-damage design spectra for reinforced concrete structures," *Earthquake Engineering and Structural Dynamics*, vol. 33, no. 12, pp. 1211–1231, 2004.

[39] J. M. Nau and W. J. Hall, *An Evaluation of Scaling Methods for Earthquake Response Spectra*, University of Illinois Engineering Experiment Station, Champaign, IL, USA, 1992.

[40] E. Miranda, "Evaluation of site-dependent inelastic seismic design spectra," *Journal of Structural Engineering*, vol. 119, no. 5, pp. 1319–1338, 1993.

[41] M. Ordaz and L. E. Pérez-Rocha, "Estimation of strength-reduction factors for elastoplastic systems: a new approach," *Earthquake Engineering and Structural Dynamics*, vol. 27, no. 9, pp. 889–901, 1998.

[42] C. Zhai, D. Ji, W. Wen, W. Lei, and L. Xie, "Constant ductility energy factors for the near-fault pulse-like ground motions," *Journal of Earthquake Engineering*, vol. 21, no. 2, pp. 343–358, 2017.

[43] A. K. Chopra, *Dynamics of Structures: Theory and Applications to Earthquake Engineering*, Prentice Hall, Englewood Cliffs, NJ, USA, 4th edition, 2012.

[44] R. S. Jalali and M. D. Trifunac, "A note on strength-reduction factors for design of structures near earthquake faults," *Soil Dynamics and Earthquake Engineering*, vol. 28, no. 3, pp. 212–222, 2008.

[45] C. Zhai, D. Ji, W. Wen, C. Li, W. Lei, and L. Xie, "Hysteretic energy prediction method for mainshock-aftershock sequences," *Earthquake Engineering and Engineering Vibration*, vol. 17, no. 2, pp. 277–291, 2018.

[46] C. Adam, L. F. Ibarra, and H. Krawinkler, "Evaluation of *P*-delta effects in nondeteriorating MDOF structures from equivalent SDOF systems," in *Proceedings of the 13th World Conference on Earthquake Engineering*, vol. 3407, Vancouver, Canada, August 2004.

[47] A. Gupta and H. Krawinkler, "Seismic Demands for Performance Evaluation of Steel Moment Resisting Frame Structures," Stanford University, Stanford, CA, USA, 1999.

[48] S. H. Hwang and D. G. Lignos, "Earthquake-induced loss assessment of steel frame buildings with special moment frames designed in highly seismic regions," *Earthquake Engineering and Structural Dynamics*, vol. 46, no. 13, pp. 2141–2162, 2017.

[49] K. Levenberg, "A method for the solution of certain nonlinear problems in least squares," *Quarterly of Applied Mathematics*, vol. 2, no. 2, pp. 164–168, 1944.

[50] D. W. Marquardt, "An algorithm for least-squares estimation of nonlinear parameters," *Journal of the Society for Industrial and Applied Mathematics*, vol. 11, no. 2, pp. 431–441, 1963.